High Angle-of-Attack Aerodynamic Characteristics

of Crescent and Elliptic Wings

by

C. P. van Dam

University of California, Davis, CA
Department of Mechanical Engineering
Division of Aeronautical Science and Engineering

Final Report

May 1989

Abstract

Static longitudinal and lateral-directional forces and moments were measured for elliptic-and crescent-wing models at high angles of attack in the NASA Langley 14- By 22-Ft Subsonic Tunnel. The forces and moments were obtained for an angle-of-attack range including stall and post-stall conditions at a Reynolds number based on the average wing chord of about 1.8 million. Flow-visualization photographs using a mixture of oil and titanium-dioxide were also taken for several incidence angles. The force and moment data and the flow-visualization results indicated that the crescent wing model with its highly swept tips produced much better high-angle-of-attack aerodynamic characteristics than the elliptic model. Leading-edge separation-induced vortex flow over the highly swept tips of the crescent wing is thought to produce this improved behavior at high angles of attack. The unique planform design could result in safer and more efficient low-speed airplanes.

Nomenclature

AR	-	aspect ratio, b^2/S
b	-	wing span [ft]
c	-	chord length [ft]
c_{av}	-	average chord length, S/b [ft]
c_l	-	sectional lift coefficient, lift per unit span/$(q_\infty c)$
c_r	-	root chord length [ft]
C_L	-	lift coefficient, lift/$(q_\infty S_{ref})$
$C_{L,\alpha}$	-	lift curve slope, $\partial C_L/\partial \alpha$ [per deg]
C_l	-	rolling moment coefficient, rolling moment/$(q_\infty S_{ref} b_{ref})$
C_m	-	pitching moment coefficient, pitching moment/$(q_\infty S_{ref} c_{ref})$
$C_{m,\alpha}$	-	slope of pitching-moment-coefficient curve, $\partial C_m/\partial \alpha$ [per deg]
C_n	-	yawing moment coefficient, yawing moment/$(q_\infty S_{ref} b_{ref})$
q_∞	-	freestream dynamic pressure [lb/ft^2]
S	-	wing area [ft^2]
y	-	spanwise distance from wing root [ft]
α	-	angle of attack [deg]
β	-	sideslip angle [deg]
η	-	nondimensional spanwise station, $y/(b/2)$

Subscripts:

max	-	maximum
ref	-	reference

Introduction

In 1971, Küchemann discussed the possibility of designing wings that combine vortical flows with classical attached flows.[1] While admitting "that such designs must be more risky and are more likely to fail," Küchemann suggested that the benefits justified abandonment of the classical concept of maintaining flow over the entire wing throughout the whole flight regime.[2] This idea of combined vortex flows and classical attached flows has been integrated in the wing design of highly maneuverable military aircraft; all current generation fighter aircraft make use of this concept in one way or the other. However, in the design of low speed and transport aircraft, the concept of maintaining attached flow over the entire wing throughout the flight regime (from cruise to near stall) has been adhered to. In this philosophy, flow separation is avoided - sometimes at great cost - until angles of attack close to stall, when trailing-edge separation is designed to occur over the inboard portion of the wing. The outboard region of the wing is designed to maintain attached flow until post-stall angles of attack to maximize roll stability and control and to minimize the chances of stall-spin entry.

To meet the design objectives in the framework of the classical attached-flow approach several options are available. First, wing sweep is kept to a minimum to reduce tip loading and, thus, the danger of tip stall. Conventional aft sweep puts the outboard portion of the wing in the upwash field of the inner part of the wing and, as a result, the outer part carries more lift for a given angle of attack. Flow separation over the tip region must be minimized; therefore, the wing is swept only as required to minimize the compressibility drag rise at cruise conditions. Wing twist can also be applied to reduce the

aerodynamic loading over the outboard portion of a swept or unswept wing. However, a significant induced-drag penalty at cruise often results because of deviations from an optimal spanwise-load distribution. Wing section shape can be varied in the spanwise direction with high $c_{l,max}$-airfoils employed in the outer wing region. This design option may result in a viscous drag penalty at cruise conditions because airfoil performance at these conditions is sacrificed to improve the high-angle-of-attack lifting characteristics. Wing tip chords are designed to be sufficiently large to avoid low tip-chord Reynolds numbers and the attendant difficulties with flow separation. Finally, wing leading-edge modifications such as slots, slats, or flaps can be incorporated to improve the aerodynamic characteristics of wings at high-angle-of-attack. These systems often result in increased complexity, maintenance, cost and sometimes in degraded aerodynamic cruise performance. In recent years, the fixed outboard leading-edge droop has proven to significantly increase the stall departure and spin resistance of low-speed aircraft.[3] Although geometrically simple, this modification may result in reduced aerodynamic performance at cruise conditions. Also, for wings with a relatively blunt leading edge or for high-aspect-ratio wings, a leading-edge droop is not always effective to increase stall departure and spin resistance.

In this report, a crescent wing planform which combines attached flow over the inboard portion of the wing with vortical flow over the outboard portion of the wing is examined experimentally.[4] Wing sweep is used to induce separation along the rounded leading-edge of the outboard wing region. The resulting vortical flow over this portion of the wing produces a significant amount of lift and, consequently, improved lateral stability and controllability at stall and post-stall conditions. Also, the wing tip with vortex flow tends to

generate a nose-down pitching moment at stall. However, at cruise and climb conditions the flow must be attached over the entire wing to minimize drag. It should be noted that the highly swept tip concept can also be beneficial for wings of high-speed airplanes[5] and blades of helicopters[6]. This report presents the results of a wind-tunnel experiment which was conducted to evaluate this design concept for moderate-to-high aspect ratio wings first introduced in Ref. 4 (also see Ref. 7).

Experiment

A wind-tunnel experiment was conducted in the NASA Langley 14- By 22-Ft Subsonic Tunnel to investigate the influence of wing planform shape on the high-angle-of-attack aerodynamic characteristics. In Fig. 1, a plan view is shown of the elliptic and crescent wing configurations investigated. Fig. 2 provides a photograph of the model and the sting mount used in the present test. Both wings had identical wing area ($S = 6.47$ ft^2), wing span ($b = 6.74$ ft), spanwise chord distribution (constant for center panel and elliptic for outboard panel), aspect ratio (AR=7), and airfoil section shape in the freestream direction (NACA 0012). Also, the models had zero wing twist and zero dihedral. The only difference between the two models was the planform shape. The crescent wing had a quarter-chord line which is curved rearward, whereas the elliptic wing had a straight, unswept quarter-chord line. The center body (body diameter is 5 in.) and the center wing panel (see Fig. 1) were obtained from an existing variable-wing-twist model.[8] This dictated the root chord length and section shape for the outboard wing panel.

The crescent shape was originally developed to investigate induced drag and is a further development of wings with discontinuous sheared tips.[4,9]

Calculations[10] and preliminary wind-tunnel results indicate that the crescent wing shape generates a lower induced drag than the classical unswept elliptic wing for a given lift and span at attached-flow conditions.

The dynamic pressure and the unit-Reynolds number of the freestream during the measurements were approximately 100 lb/ft^2 and 1.85 million/ft, respectively. For the average chord of slightly less than 1 ft, a test Reynolds number of 1.8 million was realized. The rounded leading edge of the wing maximizes the leading-edge suction force and, thus, the performance at cruise and climb conditions. The separation-induced vortex flow is very much Reynolds number dependent for wings with a rounded leading edge.[11] The test Reynolds number was maximized to obtain values that approached the range of Reynolds numbers encountered by low-speed aircraft at high lift coefficients and to avoid low Reynolds-number flow behavior which could have made the results different to interpret. The force-and-moment measurements for both configurations were obtained with a six-component balance mounted in the model center body (Fig. 2).

Boundary-layer transition was fixed on both models at 5% of the chord (in the freestream direction) over the upper and lower surfaces along the entire span. The width of the trip strips was 0.125 in. Over the crescent-wing model, attachment-line trip strips were located around the leading edge at about $\eta = \pm$ 0.98 (Fig. 3). These trips were oriented normal to the leading edge to ensure transition of the leading-edge attachment-line boundary layer along the highly swept tips at low angles of attack.[12] On the center body the transition was fixed circumferentially at 3.0 in. downstream of the nose.

The models were tested for an angle-of-attack range from 0° to 21° (tunnel constraint) at zero sideslip angle. Also, force and moment measurements were

made for an angle-of-sideslip variation from 0° to 15°, 15° to -15°, and -15° to 0° at several angles of attack.

Wind-off tares were carefully determined after each change in configuration. At each incidence angle, balance readings were taken over a period of 10 sec at a rate of 5 readings/sec. In the following figures each experimental data point represents the average value of these readings. The repeatability of the data is exemplified by the comparisons shown in Fig. 4. In Fig. 4, lift and pitching-moment results obtained during two separate data runs are compared for the crescent configuration. The comparisons of the data demonstrate good repeatability even at stall and post-stall conditions.

Surface oil flow visualizations were conducted to study the behavior of the boundary layer. A mixture of light mineral oil and titanium dioxide was used to visualize the surface streak lines. The visualizations were conducted at the test Reynolds number and several angles of attack.

Results

In this section, the effects of wing planform on high angle of attack behavior are illustrated by comparing the lift and static-stability characteristics and the flow visualizations for both configurations. The moments were measured with respect to a fixed point on the model center line, located longitudinally and vertically at the $0.25c_r$ location (3.5 in. aft of the leading edge). The lateral-directional moments were referred to the body-axis system with the origin located at the moment center. The force-and-moment coefficients were nondimensionalized by the reference wing area of 6.47 ft^2, the reference wing span of 6.74 ft, and the reference chord (c_{av}) of 0.96 ft.

Forces and Moments

In Figs. 5 through 6, the measured lift, and pitching-moment curves for both configurations are presented. The lift characteristics for both wings were virtually identical for low angles of attack (α < 6°) as shown in Fig. 5a. At higher angles of attack the crescent wing produced slightly less lift for a given incidence angle (Figs. 5a and 5b). A dramatic change occurred at α = 13° and C_L = 0.98. At these test conditions, the elliptic wing reached its maximum lift condition whereas lift continued to increase for the crescent wing (Fig. 5b). The crescent wing reached a maximum lift coefficient $C_{L,max}$ = 1.06 at α = 14.5°. The post-stall behavior of the crescent wing was steady and benign; however, the elliptic wing displayed a much more abrupt and unsteady post-stall behavior. This difference in stall and post-stall characteristics is also exhibited in the lift data of Fig. 5b. The post-stall reductions in lift were nearly linear for the crescent configuration whereas they were very nonlinear for the elliptic configuration.

The pitching-moment results are presented in Fig. 6. The pitching-moment coefficients for zero-angle-of-attack were identical for both wings. At low angles of attack, the pitching-moment coefficient slope with angle of attack $C_{m,\alpha}$ was about zero for the elliptic wing; i.e. the aerodynamic center was about located near the moment center, as expected. The crescent wing displayed a linear and stable $C_{m,\alpha}$ behavior until high angles of attack; $C_{m,\alpha}$ = -0.014 deg^{-1} at low angles of attack indicating the location of the aerodynamic center was about 0.18c_{av} downstream of the moment center. Nose-down pitching moments were much larger for the crescent wing than for the elliptic throughout the angle of attack range, including post-stall. This stabilizing effect was expected due to the tendency of the flow to stay attached on the rearward

displaced tips of the crescent wing.

In Figs. 7 and 8 the lateral-directional results are presented for angles of attack ranging from 0° to stall. The rolling-moment coefficient due to sideslip (dihedral effect) exhibited a stable trend for both the elliptic (Fig. 7a) and crescent model (Fig. 7b). The lateral stability of the elliptic configuration was marginal for incidence angles below stall (α = 0°, 7°, and 12°) and pronounced at the post-stall condition (α = 14°). The crescent configuration with the highly swept tips displayed increased lateral stability as compared to the elliptic configuration, as expected.[9] The lateral-directional characteristics of the crescent wing were only obtained at pre-stall conditions (α = 0°, 7°, and 14°).

The yawing-moment coefficient due to sideslip was nearly identical for both wings at low-to-moderate angles of attack (Figs. 8a and 8b). At high but pre-stall angles of attack directional stability became positive for both the elliptic (Fig. 8a, α = 12°) and the crescent model (Fig. 8b, α = 14°). The crescent wing configuration, expecially, displayed a very stable behavior for small deviations in sideslip angle at this condition.

Flow Visualizations

Extensive flow visualization tests on the upper surface (the suction side) of the wings were conducted at various angles of attack. The results are summarized in Figs. 9 and 10 for the elliptic and the crescent configuration, respectively. In Figs. 9a and 9b surface flow patterns in the form of titanium-dioxide streak lines are visible for the elliptic wing at a cruise/climb condition (α = 7°). The flow pattern was very symmetric; the streak lines ran nearly parallel to the longitudinal axis of the model. No

separation or vortex action was detectable in the oil flow pattern near the wing tip at these conditions (Fig. 9b). The results for the crescent wing at the identical conditions are shown in Figs. 10a and 10b. The flow pattern was symmetric but in the tip region the streak lines displayed a strong outward curvature at this angle of attack. This boundary-layer behavior resulted in limited "premature" trailing-edge separation at slightly higher angles of attack and explains the slight reduction in $C_{L,\alpha}$ at those conditions (Fig. 5).

The results for $\alpha = 14°$ are displayed in Figs. 9c and 10c. The flow over the crescent wing was still attached except for the tip trailing-edge region at this (for the crescent wing) pre-stall condition (Fig. 10c). However, at this angle of attack the elliptic wing had stalled and an asymmetric flow pattern had developed (Fig. 9c). A slight variation in the flow angularity across the wind-tunnel test section caused the left wing to stall first. Consequently, the post-stall flow patterns remained somewhat asymmetric. In Fig. 9c, the separated flow patterns across the tip regions of the elliptic model are clearly visible. The flow across the inboard portion of the wing was still attached at these conditions. This tip stall appears to explain the abrupt and unsteady behavior of the elliptic wing at these conditions.

At $\alpha \geq 15°$, both the elliptic and the crescent model had stalled and both displayed asymmetric flow patterns. However, the flow across the elliptic wing was completely separated (Fig. 9d), whereas the tips of the crescent wing exhibited attached flow at these conditions (Figs. 10d through 10g). Especially note the vortical patterns across the highly swept wing tips. This vortical flow pattern appears to explain the benign and steady stall behavior of the crescent wing and the increment in lift at stall and post-stall conditions. Furthermore, these results illustrate the beneficial effect of the

highly three-dimensional flow on the wing-tip characteristics. Specifically, the tip of the crescent wing maintains attached flow at conditions for which the tip of the elliptic wing separates. This result indicates that wing tips can be designed with small tip-chord Reynolds numbers, by taking advantage of such three-dimensional flow behavior.

Concluding Remarks

A wind-tunnel experiment was conducted to explore the differences in high-angle-of-attack characteristics of crescent compared to elliptic wing planforms. On a crescent wing, sweep is used to induce separation along the rounded leading-edge of the outboard wing region. The resulting vortical flow over this portion of the wing produces a significant amount of lift and, therefore, stability and controllability at stall and post-stall angles of attack. At cruise and climb conditions the flow is kept attached over the entire wing to maximize the leading-edge suction force and, thus, minimize the drag force. This study served to evaluate this concept of combined vortex and attached flows for overall improved wing behavior.

Forces and moments were measured and surface flow visualizations were conducted to compare the aerodynamic characteristics of crescent and elliptic wing planforms at high angles of attack. The wind-tunnel results indicated that the crescent wing model with its highly swept tips had much better high-angle-of-attack aerodynamic characteristics than the unswept elliptic wing model: 1) $C_{L,max}$ was 8% higher for the crescent wing; 2) post-stall lift and pitching-moment behavior was improved for the crescent wing; 3) dihedral effect of the crescent wing was stronger and more linear than the elliptic wing. The flow visualization revealed the existence of vortical flow patterns across the

highly swept tips of the crescent wing.

These results indicate the potential for improved wing-tip aerodynamics by taking advantage of this three-dimensional flow behavior to control separation on surfaces with low tip-chord Reynolds numbers. Also, these experimental results appear to validate the design concept of combining leading-edge separation-induced vortex flows and attached flows for improved behavior for moderate aspect ratio wings at high angles of attack.

More detailed experiments, including pressure measurements, are necessary to further explore the static and dynamic aerodynamic characteristics of these wings with highly swept tips at stall and post-stall conditions.

References

1. Küchemann, D., "On the Possibility of Designing Wings that Combine Vortex Flows with Classical Aerofoil Flows," RAE TM Aero 1363, Oct. 1971.

2. Küchemann, D., The Aerodynamic Design of Aircraft, Pergamon, 1978.

3. Staff of Langley Research Center, "Exploratory Study of the Effects of Wing-Leading-Edge Modifications on the Stall/Spin Behavior of a Light General Aviation Airplane," NASA TP 1589, Dec. 1979.

4. van Dam, C. P., "Swept Wing-Tip Shapes for Low-Speed Airplanes," SAE paper 851770, Oct. 1985.

5. Robins, A. W., et al., "Concept Development of a Mach 3.0 High-speed Civil Transport," NASA TM 4058, Sept. 1988.

6. Wanstall, B., "BERP Blades-Key to the 200 Kn Helicopter, "Interavia, March 1986, pp. 322-324.

7. van Dam, C. P., "Aircraft Stall-Spin Entry Deterrent System," U.S. Patent No. 4,776,542, Oct. 11, 1988.

8. Holbrook, G. T., Morris Dunham, D., and Greene, G. C., "Vortex Wake Alleviation Studies with a Variable Twist Wing," NASA TP 2442, Nov. 1985.

9. Vijgen, P.M.H.W., van Dam, C. P., and Holmes, B. J., "Sheared Wing-Tip Aero-dynamics: Wind-Tunnel and Computational Investigation," Journal of Aircraft, Vol. 26, March 1989, pp. 207-213.

10. van Dam, C. P., "Induced-Drag Characteristics of Crescent-Moon-Shaped Wings," Journal of Aircraft, Vol. 24, Feb. 1987, pp. 115-119.

11. Henderson, W. P., "Studies of Various Factors Affecting Drag due to Lift at Subsonic Speeds," NASA TN D-3584, Oct. 1966.

12. Poll, D.I.A., "Transition in the Infinite Swept Attachment Line Boundary Layer," The Aeronautical Quarterly, Vol. 30, Nov. 1979, pp. 607-629.

b = 6.74 ft

Center panel

Tunnel sting

Center panel

Tunnel sting

$c_r = 1.17$ ft

0.25 c line

0.60 ft

Unswept elliptic wing

b/2 = 3.37 ft

$c_r = 1.17$ ft

0.25 c line

1.75 ft

0.60 ft

Crescent elliptic wing
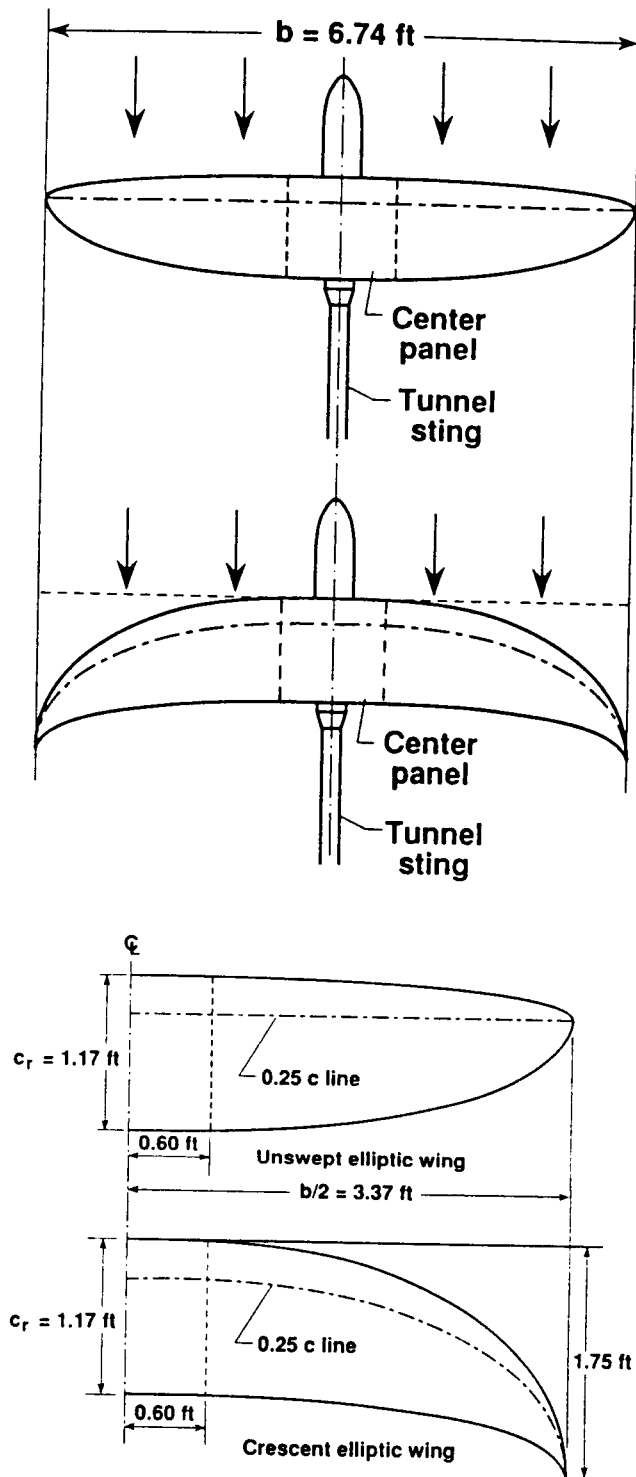
Fig. 1   Planform geometry of crescent and elliptic wind-tunnel models.
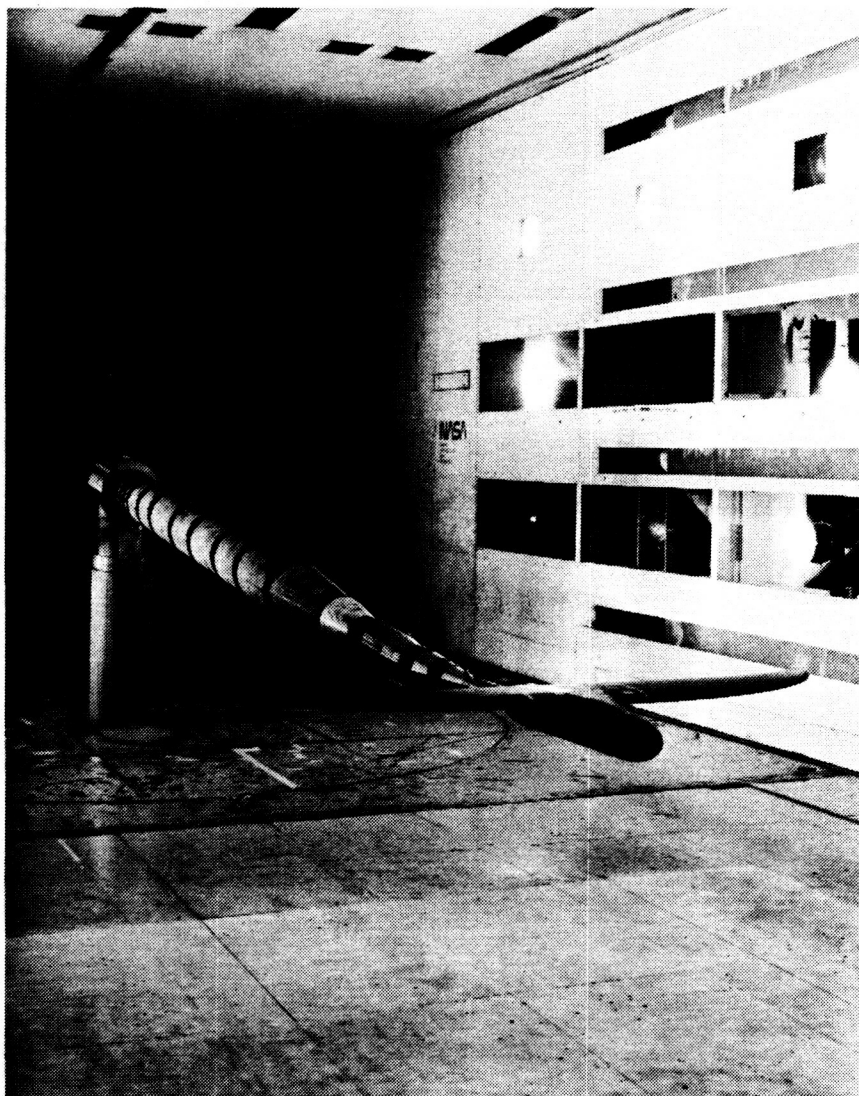
Fig. 2   Photo of crescent model in test section of the 14- By 22-Ft Subsonic
Tunnel.

0.90   0.95   1.0 $\eta = y/(b/2)$

Leading edge

Grit trip

Grit trip
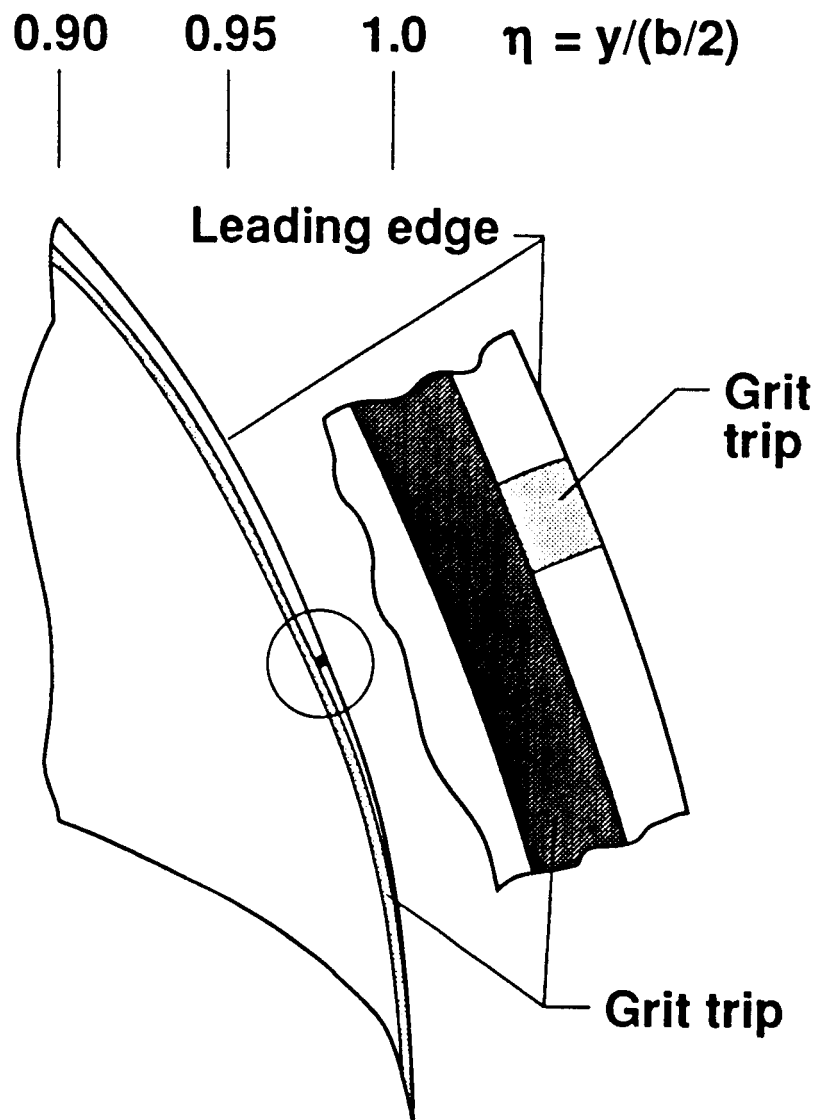
Fig. 3   Leading-edge boundary-layer transition trip on crescent wing.
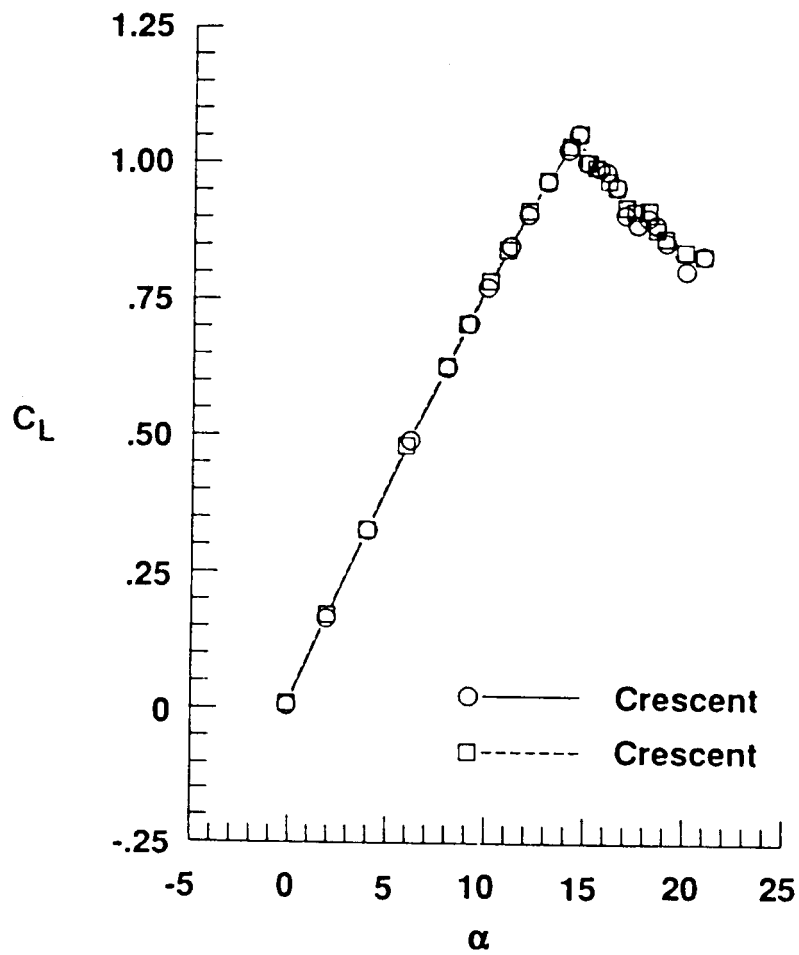
(a) Lift curve ($\alpha = 0° - 21°$)

Fig. 4   Comparison of results for two separate data runs (crescent model).
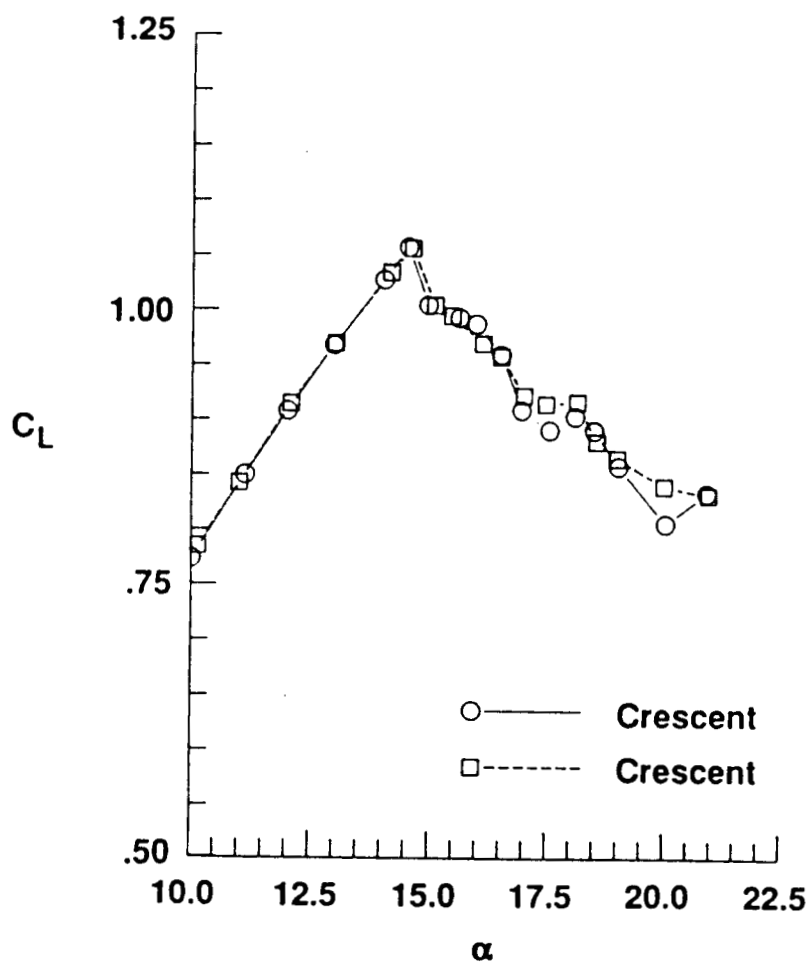
(b) Lift curve ($\alpha = 10° - 21°$)

Fig. 4   Continued.
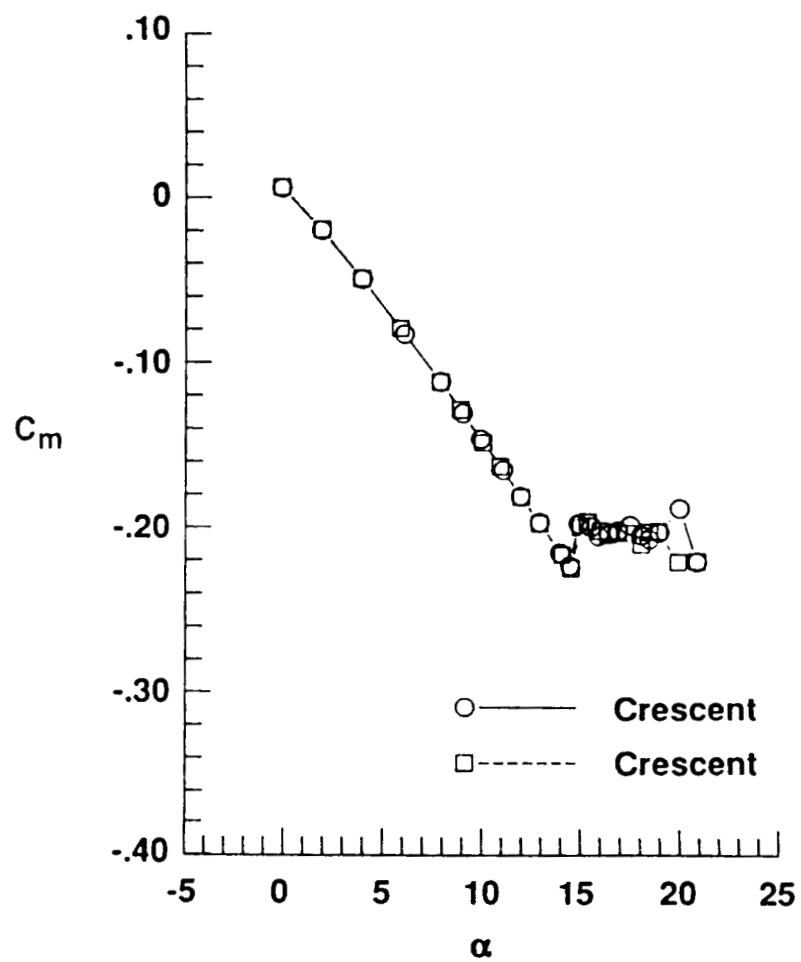
(c) Pitching moment curve

Fig. 4   Concluded.
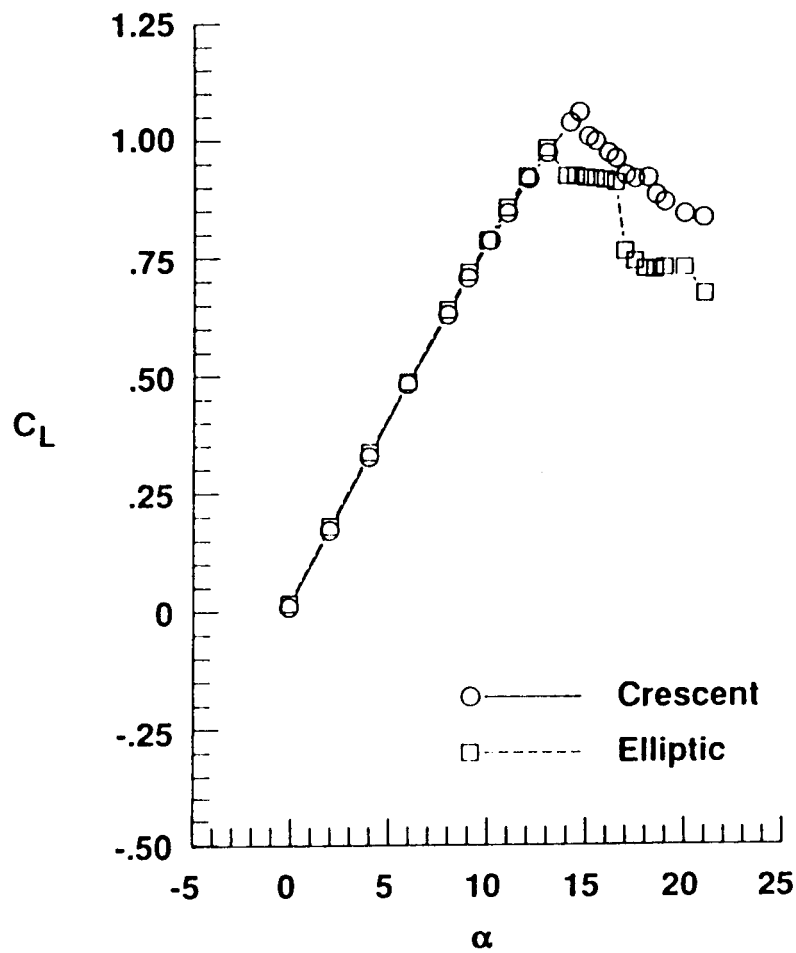
(a) $\alpha = 0° - 21°$

Fig. 5   Lift curves of elliptic and crescent model.
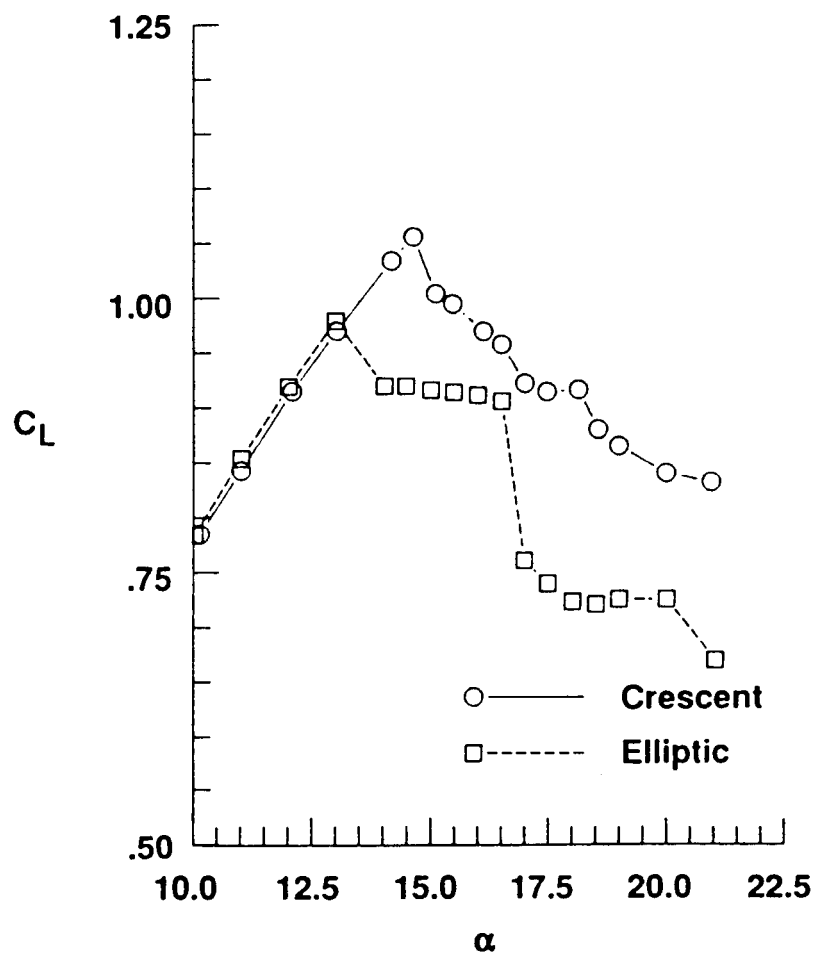
(b) $\alpha = 10° - 21°$

Fig. 5   Concluded.
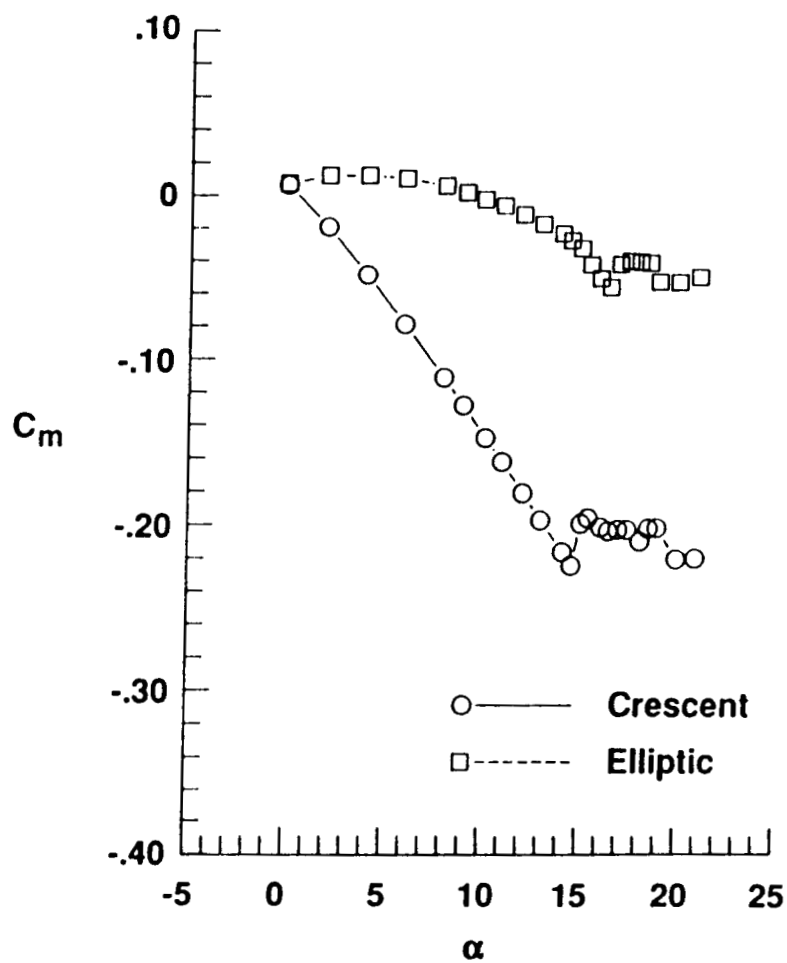
Fig. 6   Pitching moment data of elliptic and crescent model.
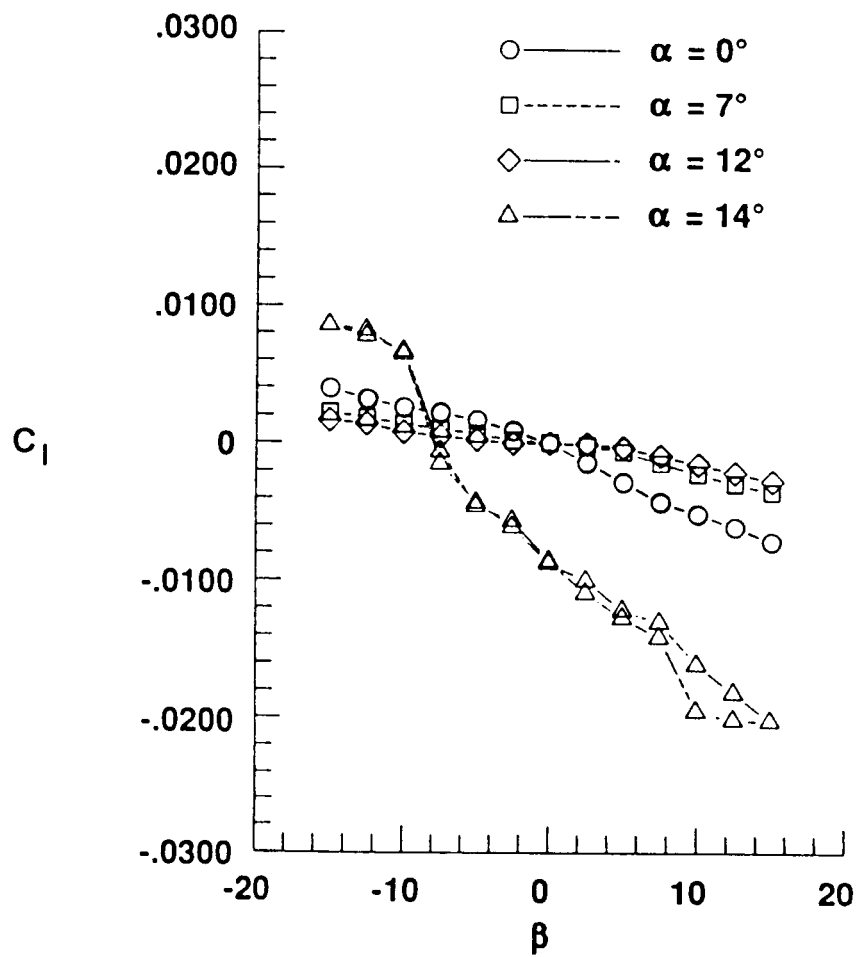
(a) Elliptic model

Fig. 7   Influence of angle of attack on lateral stability.
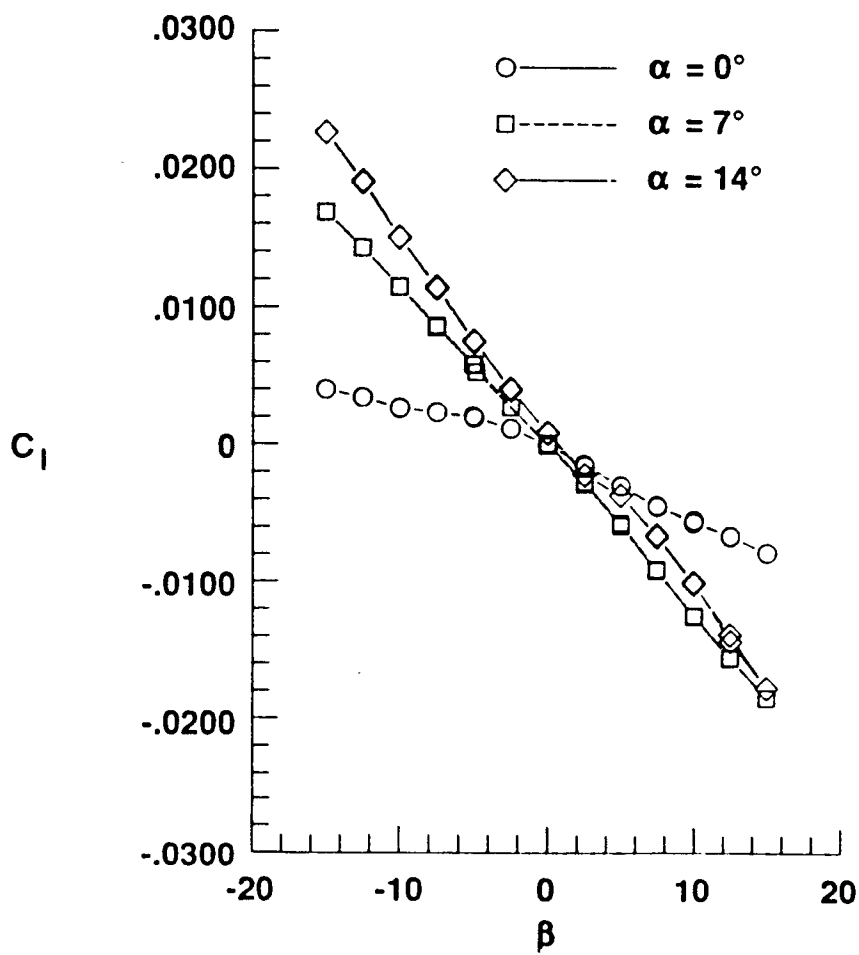
(b) Crescent model

Fig. 7   Concluded.
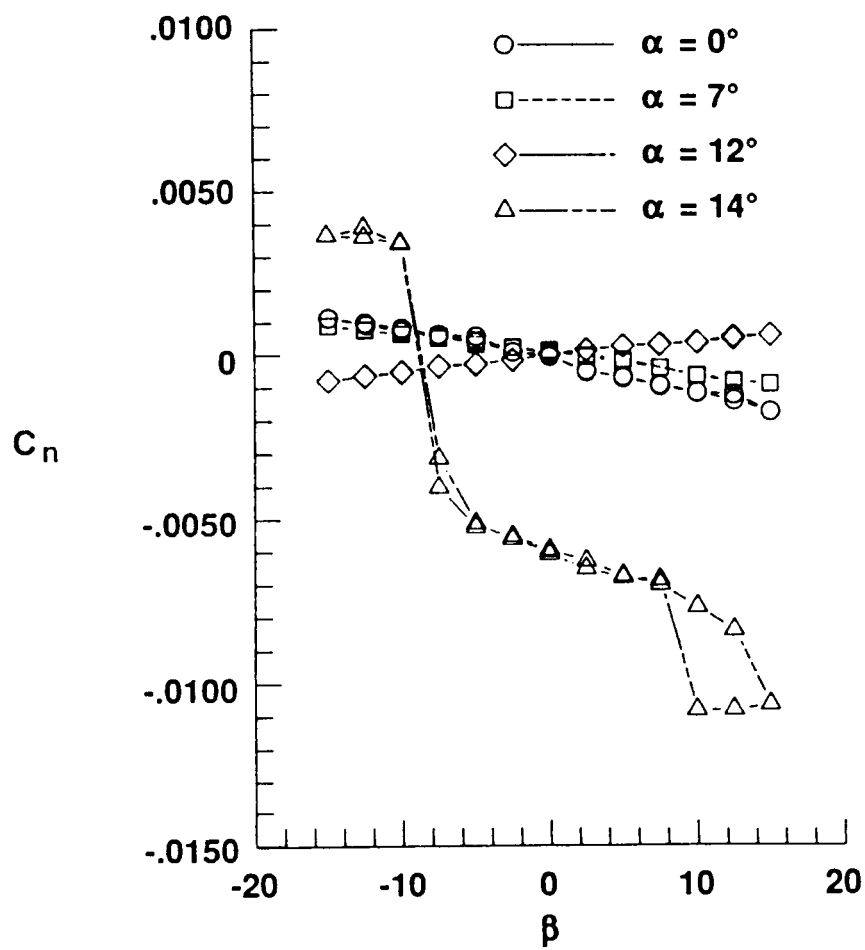
(a) Elliptic model

Fig. 8   Influence of angle of attack on directional stability.
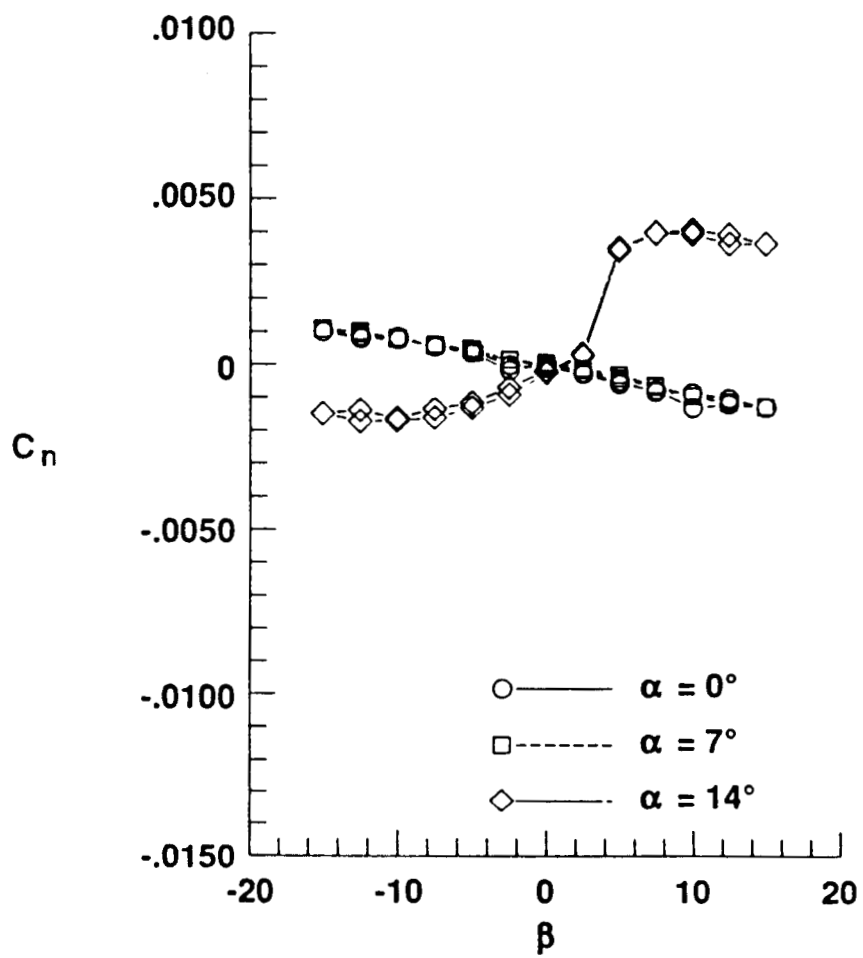
(b) Crescent model

Fig. 8   Concluded.

(a) $\alpha = 7°$

Fig. 9   Titanium-dioxide streak-line patterns over elliptic wing (freestream direction from bottom to top, $\beta = 0°$).

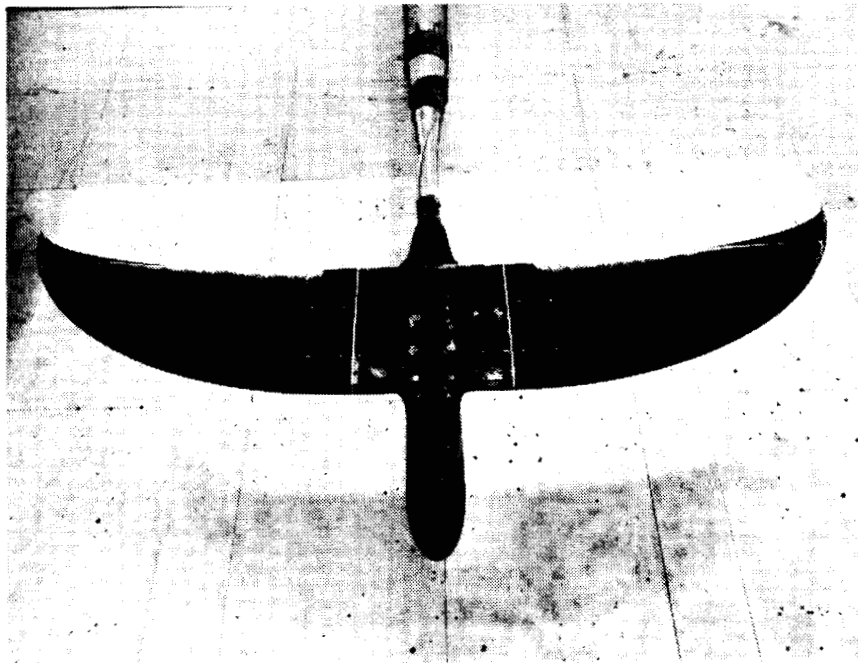(b) $\alpha = 7°$

Fig. 9   Continued.

(c) $\alpha = 14°$

Fig. 9   Continued.

(d) $\alpha = 21°$
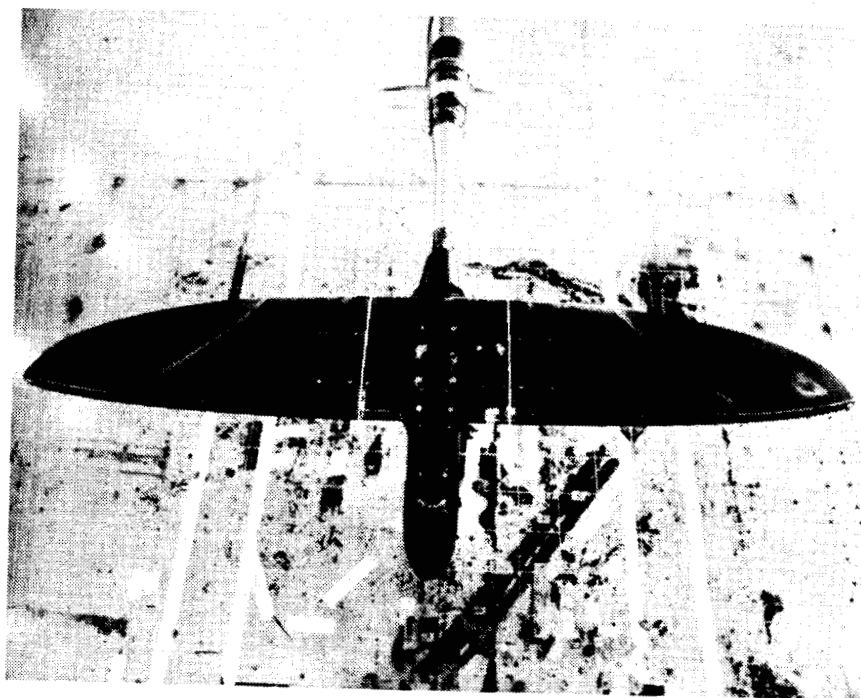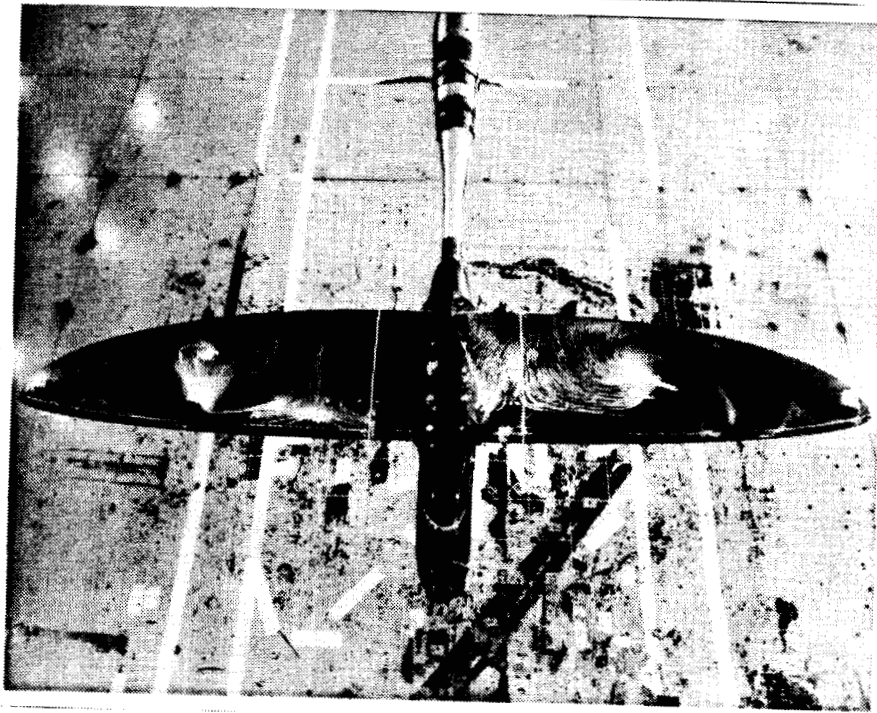
Fig. 9   Concluded.
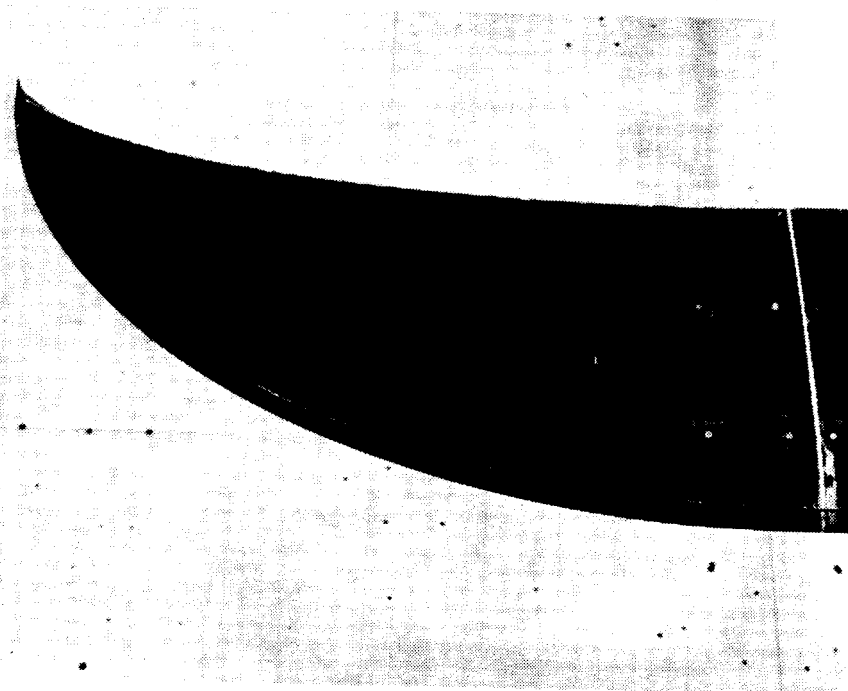
(a) $\alpha = 7°$

Fig. 10   Titanium-dioxide   streak-line   patterns   over   crescent   wing
(freestream direction from bottom to top, $\beta = 0°$).

(b) $\alpha = 7°$

Fig. 10   Continued.

(c) $\alpha = 14°$

Fig. 10   Continued.

(d) $\alpha = 16°$

Fig. 10   Continued.

(d) $\alpha = 16°$

Fig. 10   Continued.

(f) $\alpha = 21°$

Fig. 10   Continued.

(g) $\alpha = 21°$

Fig. 10   Concluded.